Hindawi
Advances in Civil Engineering
Volume 2018, Article ID 6124809, 13 pages
https://doi.org/10.1155/2018/6124809

Research Article

Effects of Initial Shear Stress and Vibration Frequency on the Dynamic Pore-Water Pressure of Saturated Sands

Jian Zhang,[1] **Jiuting Cao**,[2] **and Sijie Huang**[3]

[1]*School of Architectural Engineering, Nanjing Institute of Technology, Nanjing 211167, China*
[2]*Jiangsu Zhongshe Group Co., Ltd., Wuxi 214072, China*
[3]*Tianjin Research Institute for Water Transport Engineering, Tianjin 300456, China*

Correspondence should be addressed to Jian Zhang; 18626439990@163.com

Received 3 July 2018; Revised 5 October 2018; Accepted 25 October 2018; Published 14 November 2018

Academic Editor: Castorina S. Vieira

The cyclic triaxial system is used to investigate the effects of confining pressure, initial shear stress, vibration frequency, and dynamic stress on the pore-water pressure characteristics of saturated sand in the Wenchuan area. Results show that the initial shear stress has a remarkable effect on the development of the dynamic pore-water pressure of saturated sand. The greater the initial shear stress, the slower the development curve of the pore-water pressure of saturated sand and the higher the number of cycles required to reach the same pore-water pressure. The larger the initial shear stress, the smaller the dynamic pore-water pressure when the sample is destroyed. Moreover, the maximum pore-water pressure ratio decreases linearly with the increase of the consolidation ratio. The normalised relationship curve between the dynamic pore-water pressure and failure time of vibration is consistent with the development law of the power function. The power function model parameters are affected by the initial shear stress and confining pressure. At the time of isotropic consolidation, the accumulation law of pore-water pressure presents a growth pattern of "fast-stable-intensified." A modified pore-water pressure model considering vibration frequency is proposed on the basis of the Seed pore-water pressure model, and the model parameters are linear with the vibration frequency. When the vibration frequency remains unchanged, the parameter does not change with the confining pressure and dynamic stress. This modified model can predict the change rule of pore-water pressure with the frequency under isotropic consolidation.

1. Introduction

China is an earthquake-prone country with a wide distribution of earthquakes. In the past 100 years, the number of strong earthquakes ($M \geq 8$) in China has reached 10, with serious casualties and property losses in densely populated areas. A large number of earthquakes indicate that the liquefaction of saturated sand has caused great damage to pile foundations, embankments, slopes, and dams [1]. Prior to the onset of seismic loads, the foundations of these structures are often subjected to initial shear stress due to the presence of upper structures [2, 3]. Figure 1 shows that the initial shear stress of the soil unit at A is zero, the isotropic consolidation is simulated in the dynamic triaxial test, and the equal consolidation pressure is applied. The initial shear stress of the soil unit at B is not equal to zero, and the unequal pressure consolidation method can be used to simulate the stress state before the earthquake [3–5].

Most tests at present mainly consider the state where the initial shear stress does not exist; that is, starting the test based on the equal 3D consolidation pressure. The initial shear stress is an important factor affecting the dynamic properties of saturated sand, and numerous researchers are beginning to focus on studying the effect of initial shear stress [6–10].

Several scholars have studied the development law of pore-water pressure under cyclic loading, the most famous among which was finished by Seed and Idriss [11]. They obtained the relationship curve between the pore-water pressure and vibration ratios on the basis of isobaric conditions through the undrained dynamic triaxial test. They also proposed a pore-water pressure development model, namely, Seed pore-water pressure development curve. The

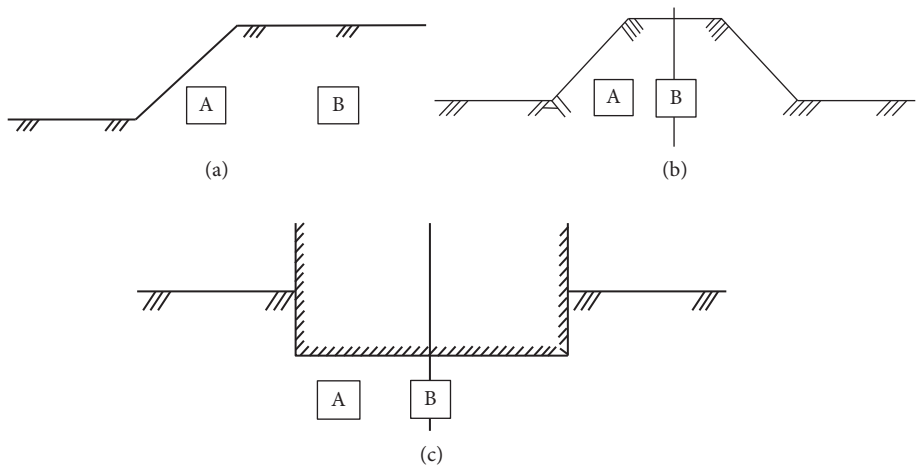

Figure 1: Initial shear stress exists in B and not in A.

growth trend of dynamic pore-water pressure was different from that of the isotropic consolidation test when the initial shear stress exists. In the nonisotropic consolidation tests, as the consolidation ratio increased, the growth rate of the pore-water pressure ratio decreased with the increase in the number of cycles after the pore-water pressure ratio exceeded a certain value. Therefore, the Seed pore-water pressure development model cannot reflect the development law of the pore-water pressure when the initial shear stress exists. Seed and Harder [12] observed remarkable reductions in the cyclic resistance of loose sands with increasing static shear stress, which is contrary to the enhanced resistance observed for medium-dense sands. Kato et al. [13] performed undrained triaxial compression tests on Toyoura sand and proposed that different consolidation states affect the development of pore-water pressure up to an axial strain of 5%. Beyond a strain of 10%, the sand behaviour became independent of the stress state at consolidation. Yang and Sze [14] investigated the undrained behaviour of sand in nonsymmetrical cyclic loading and observed that the initial shear stress is beneficial to the liquefaction resistance at low α levels but is determined at high α levels. Sivathayalan and Ha [15] observed a remarkable reduction on cyclic strength due to the anisotropic consolidation of a contractive subrounded silica sand for relative densities of up to 60%. Georgiannou and Konstadinou [16] investigated the response of Ottawa sand to cyclic torsional loading under different densities and proposed that the samples showed initial liquefaction at a loose state and high pore-water pressure ratio (>70%) at high densities under isotropic consolidation. The pore-water pressure of samples did not exceed 40% under anisotropic consolidation, and failure was induced by a flow-type deformation in loose samples. Suazo et al. [17] investigated the effect of initial shear stress on the liquefaction resistance of fine-grained tailings. They proposed that the initial shear stress decreases the liquefaction resistance, and the maximum pore-water pressure ratio fluctuates between 0.8 and 0.98. Pan and Yang [18] examined the combined effect of cyclic and static shears on the undrained cyclic response of sand. They presented that the relationship between the normalised residual pore-water pressure ratio and normalised number of loading cycles is not affected by the amplitude of the cyclic stress but is greatly influenced by the static shear stress. Yang and Pan [19] analyzed the undrained cyclic behaviour of saturated loose sand with the static shear under triaxial compression and extension conditions. They introduced the different static stress conditions that lead to distinct failure modes, flow liquefaction, and residual deformation failure. Gao et al. [20] conducted a series of cyclic shaft torsion coupling tests that simulated wave loads of different frequencies with the Yangtze River estuary silt. They found that the growth mode of the pore-water pressure of the silt is "fast-stable-abrupt," and they constructed a pore-water pressure growth model of silt under wave loading.

The abovementioned analyses show that earthquakes can cause damages to numerous sand foundations, and the effects of initial shear stress are inevitable on these foundations. At present, only a few dynamic pore-water pressure models of sand consider the influence of initial shear stress, and no pore-water pressure development model considers vibration frequency. Therefore, studying the development mode of the pore-water pressure of saturated sand under initial shear stress and vibration frequency, analysing the influence of initial shear stress and vibration frequency on the development law of pore-water pressure, and establishing a modified model of the dynamic pore-water pressure of saturated sand by considering vibration frequency are necessary. The findings will provide an experimental basis for the dynamic response analysis of sand under cyclic loading.

2. Soil Samples and Plans

2.1. Soil Samples. The sand used in this study was obtained from Wenchuan, Sichuan (China), and the sampling depth was approximately 5 m. During the transportation process, the disturbance of the soil sample was large, and the natural state of the sand was not properly controlled. Therefore, remoulded sand was used for the test. Table 1 shows the physical properties of the sand in the test. Figure 2 displays the sand particle size distribution curve.

Table 1: Physical properties of the test material.

Soil category	G_s	ρ_{dmax}	ρ_{dmin}	D_r	C_u	C_c
Sand	2.66	1.67	1.22	55%	3.5	0.64

2.2. Test Procedures and Methods. This test used a triaxial apparatus (DDS-70, China) and a remoulded soil sample with a diameter of 39.1 mm and a height of 80 mm. The remoulded soil sample was prepared through a multilayer wet mortar method and divided into five layers for compaction. The weight of each layer was determined on the basis of the dry density of the soil sample and the predesigned moisture content. Each layer was compacted to the corresponding height, and the contact surfaces were shaved to ensure good contact between layers. After preparation, the sample was installed in the pressure chamber of the cyclic triaxial apparatus. Figures 3 and 4 present the compaction and installation of the sample, respectively. In the pressure chamber, three methods were applied to saturate the sample, namely, vacuum pumping, airless water, and reversing pressure, thereby avoiding the disturbance of the sample when it was placed in a vacuum-saturated cylinder. When the pore-water pressure coefficient is $B \geq 0.97$, the sample was considered to meet the saturation requirement. In the consolidation phase, the drain valve was opened slowly after the sample was saturated. When the pore-water pressure dissipated close to 0, the drain valve should be closed for 5 min. When the pore-water pressure no longer increased, the consolidation was considered complete. After the isotropic consolidation, the deviatoric stress was gradually increased. At this time, the drain valve should be opened to avoid deformation and damage. When the corresponding deviatoric stress was applied, the sample was consolidated for a period of time, and then, the drain valve was closed to complete the bias consolidation process. In this study, the seismic wave was simplified to an equal amplitude sine wave for the dynamic triaxial test, and the vibration frequencies were selected to be f = 1 Hz, f = 2 Hz, and f = 3 Hz. The damage standards adopted in this study were pore-water pressure and deformation standards. The pore-water pressure standard is based on the development of pore-water pressure, and the failure standard indicates that the pore-water pressure is equal to the confining pressure. When an initial shear stress occurred, the deformation standard that achieved a single strain of 5% was adopted as the failure standard.

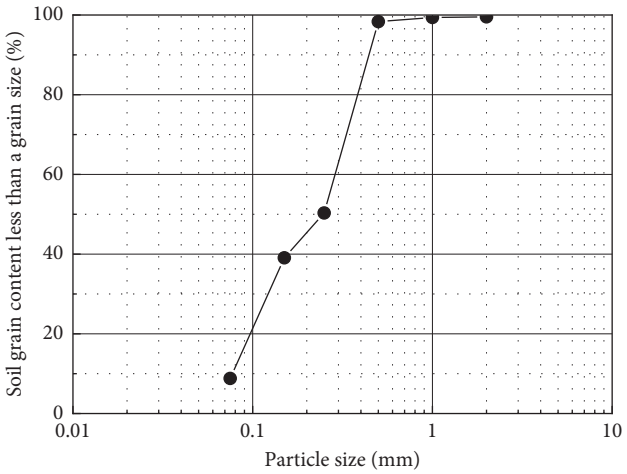

Figure 2: Particle size distribution curve.

Figure 3: Sample compaction.

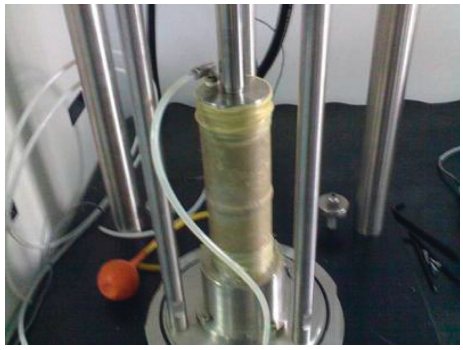

Figure 4: Sample installation.

2.3. Test Plan. On the basis of the soil extraction depth and research requirements, the consolidation confining pressures in this test are σ_{3c} = 50 kPa, σ_{3c} = 100 kPa, and σ_{3c} = 150 kPa. The drainage of the clay layer is slow due to the short acting time of the cyclic loading provided by the earthquake, which can be regarded as the soil is undrained, so the test used undrained shear. On the basis of the frequency range of seismic loading, the vibration frequencies adopted are f = 1 Hz, f = 2 Hz, and f = 3 Hz. Repeating the earthquake with the same seismic wave' waveform is impossible due to the asymmetry and irregularity of seismic loading, which is a typical random dynamic load. Therefore, the seismic loading input in this paper is simulated by the sine wave of equal amplitude waveform. Table 2 shows the specific test plan. To consider the influence of initial shear stress on the dynamic characteristics of saturated sands, the dynamic triaxial tests of consolidation ratios K_c = 1, K_c = 1.25, and K_c = 1.5 were conducted, in which

$$K_c = \frac{\sigma_{1c}}{\sigma_{3c}}, \quad (1)$$

where σ_{1c} and σ_{3c} are the vertical consolidation and confining pressures, respectively, when the sample is consolidated.

Table 2: Undrained cyclic triaxial test program of sand.

Frequency, f (Hz)	Confining pressure, σ_{3c} (kPa)	Initial shear stress, σ_s (kPa)	Vertical consolidation pressure, σ_{1c} (kPa)	Consolidation ratio, K_c	Dynamic stress, σ_d (kPa)
1, 2, 3	50	0	50	1	41, 33, 25
1, 2, 3	100	0	100	1	83, 66, 50
1, 2, 3	150	0	150	1	125, 100, 75
1	50	25	75	1.5	58, 50, 41
1	50	50	100	2	66, 58, 50, 41
1	100	50	150	1.5	108, 100, 91
1	100	100	200	2	133, 116, 100, 91
1	150	75	225	1.5	200, 150, 120
1	150	150	300	2	210, 180, 150

3. Results and Analysis

In this study, the stress model of dynamic pore-water pressure is used to establish the pore-water pressure growth models of isotropic consolidation at different frequencies and of anisotropic consolidation at a certain frequency. On the basis of the requirements of constructing the stress model of pore-water pressure, the test data are sorted and analysed to provide a basis for the future study of the characteristics of saturated sand from the perspective of the stress model.

3.1. Cyclic Response of Isotropically Consolidated Specimen. Figure 5 shows the cyclic response of the saturated sand specimen with $K_c = 1$, $\sigma_{3c} = 100$ kPa, $f = 1$ Hz, and $\sigma_d = 91$ kPa. Under isotropic consolidation ($K_c = 1$), the specimen experiences a degradation of shear stiffness and cumulative increase of pore pressure. The pore-water pressure of the specimen rapidly increases at the beginning, followed by a nearly constant rate in subsequent cycles, and the specimen is initially liquefied when the pore-water pressure reaches the confining pressure.

3.2. Effect of Initial Shear Stress on the Dynamic Pore-Water Pressure Characteristics of Saturated Sand. Figure 6(a) shows the development of the pore-water pressure of saturated sand under $K_c = 1.5$, $K_c = 2.0$, $\sigma_{3c} = 100$ kPa, $f = 1$ Hz, and $\sigma_d = 91$ kPa. The time history curves of the sample pore-water pressure are remarkably different under various initial shear stresses. Under the initial shear stress at $K_c = 1.5$, the pore-water pressure increases rapidly at first, and then, its growth rate stabilises, which later increases slightly. The strain reaches the failure standard before the pore-water pressure, and then, the sample is destroyed. Under the initial shear stress at $K_c = 2$, the pore-water pressure also increases rapidly at first, and then, it increases slowly at a relatively constant growth rate. The strain reaches the failure standard before the pore-water pressure. During cyclic vibration, the growth rate of the dynamic pore-water pressure of the sample decreases gradually due to the initial shear stress. At $K_c = 1$, the pore-water pressure ratio of the sample can reach 1.0, and the sample undergoes liquefaction destruction. At $K_c = 1.5$, the pore-water pressure ratio can reach approximately 0.6, whereas at $K_c = 2$, it can only reach approximately 0.4. In summary, the greater the initial shear stress, the slower the curve of the dynamic pore-water pressure of saturated sand, and the higher the number of cycles required to reach the same pore-water pressure. For the same number of cycles, the smaller the initial shear stress, the greater the cumulative pore-water pressure.

The curve indicates that the development of pore-water pressure can be divided into three stages. The first stage is the rapid growth phase, the second stage is the steady growth phase, and the third stage is similar to the first. The pore-water pressure undergoes various stages under the initial shear stress at different consolidation ratios. At $K_c = 1.5$, the pore-water pressure experiences all stages; at $K_c = 2$, it experiences the first and second stages. Figure 6 shows the curves of the dynamic pore-water pressure from the first to the fifth cycle, from the 40th to the 45th cycle and from the 100th to the 105th cycle, respectively, when $K_c = 1.5$, $f = 1$ Hz, and $\sigma_d = 91$ kPa.

The First Stage (the rapid growth phase). The pore-water pressure undergoes five iterations of the growth phase, as shown in Figure 6(b). The growth rate of the pore-water pressure in the first five times is 3 kPa/s, and the pore-water pressure ratio of the sample reaches approximately 0.2. The sinusoidal variation of the pore-water pressure growth process line is not remarkable. During each cycle, the pore-water pressure increases rapidly in the first half of the growth, but it decreases slightly in the second half of the decline. The main reason for this phenomenon is that after the vibration load is applied to the sample during the test, the soil particles are rearranged. Moreover, the pore-water pressure is difficult to dissipate at the initial stage of cyclic loading, thereby resulting in a large volume change potential, which leads to the rapid development of pore pressure.

The Second Stage (the steady growth phase). Figure 6(c) shows the curve of pore-water pressure from the 40th to the 45th cycle. The growth rate of the pore-water pressure per cycle is approximately 0.8 kPa/s, which is only 1/3 of the growth rate at the first stage. The pore-water pressure ratio of the sample develops to approximately 0.5 at this stage. The curve is mostly jagged, and the peak appears jagged. The pore-water pressure is lowered due to dilatancy, and the trough appears jagged. The pore-water pressure is increased due to the shearing effect, such that the sample undergoes dilatation and shearing when vibrating, thereby resulting in a jagged curve.

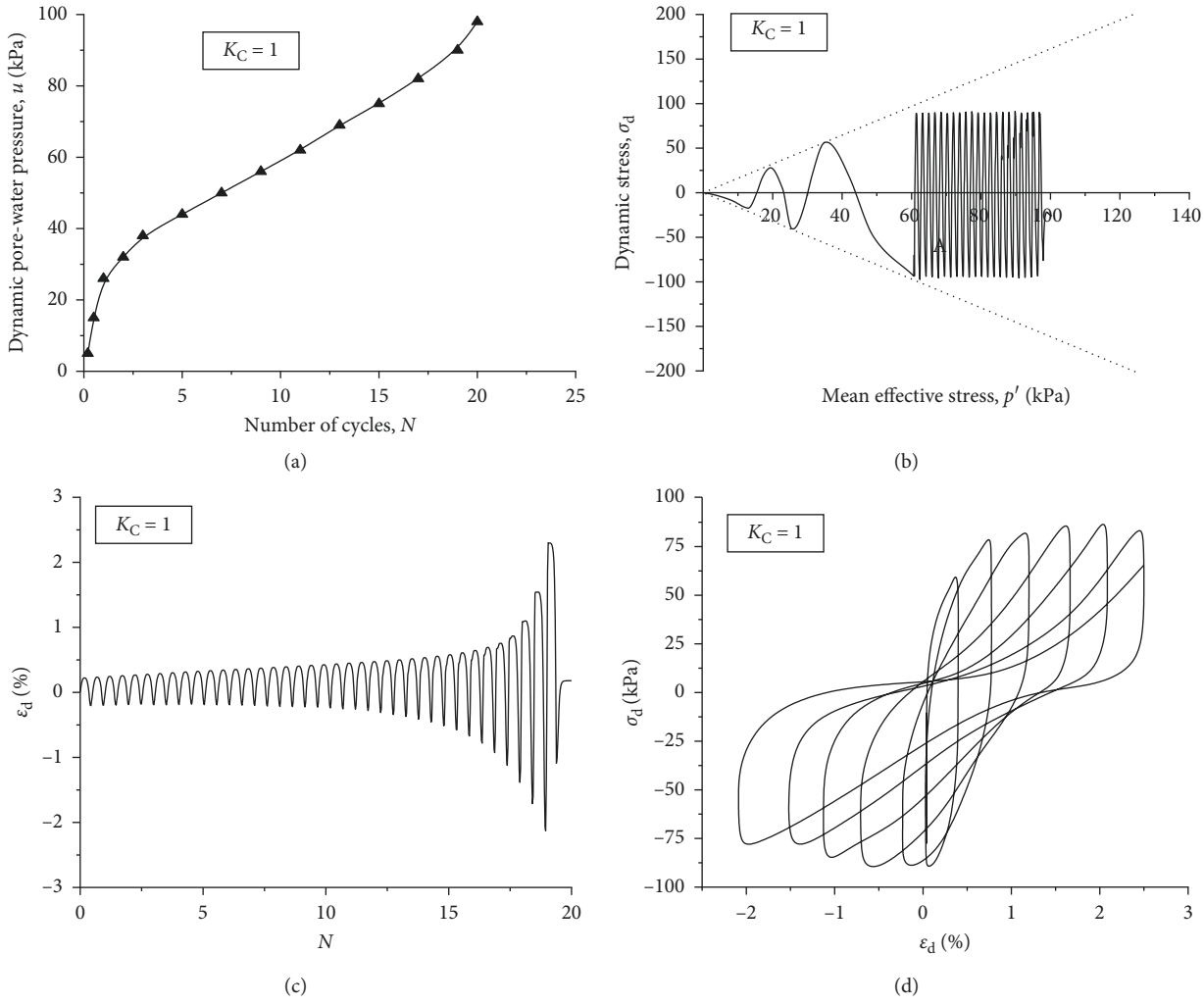

Figure 5: Undrained cyclic triaxial test on saturated sand specimens (σ_d = 91 k Pa, f = 1.0 Hz, and σ_{3c} = 100 kPa).

The Third Stage (the second rapid growth phase). From the 100th to the 105th cycle, and the growth rate of pore-water pressure increases compared with that at the second stage. Figure 6(d) shows that the growth rate per cycle of the pore-water pressure is approximately 1.4 kPa/s, which is only approximately 0.5 times that at the first stage. The pore-water pressure ratio of the sample develops to approximately 0.6 at this stage.

Figure 7 presents the relationship curve between the dynamic pore-water pressure and number of cycles under different dynamic stresses when the consolidation pressure is 50 kPa. Figure 7(a) illustrates that the dynamic pore-water pressure develops to be substantially equal to the confining pressure during isotropic consolidation. Figure 7(b) displays that, under the initial shear stress at K_c = 1.5, the dynamic pore-water pressure ratio develops to approximately 0.6 when the sample is broken during vibration. Figure 7(c) exhibits that under the initial shear stress at K_c = 2.0, the dynamic pore-water pressure ratio develops to approximately 0.4 when the sample is broken during vibration. Under the initial shear stress, the peak value of the vibrating pore-water pressure cannot reach the initial confining pressure, and the initial shear stress greatly influences the relationship curve between the pore-water pressure and number of cycles. The larger the initial shear stress, the smaller the pore-water pressure when the sample is broken.

When the maximum pore-water pressure ratio is expressed as u_{max}/σ_{3c}, the relationship curve between u_{max}/σ_{3c} and consolidation ratio K_c can be drawn. Figure 8 shows the limit pore-water pressure ratio u_{max}/σ_{3c} and consolidation ratio K_c at different consolidation ratios. When the initial shear stress exists, the dynamic pore-water pressure cannot develop to the confining pressure at the time of failure as the cycle time increases. The maximum pore-water pressure ratio when the sample is destroyed decreases linearly as the consolidation ratio increases.

The dynamic pore-water pressure and number of cycles in a curve can be processed to obtain the normalised vibration pore-water pressure and failure time of vibration curve under different consolidation ratios and confining pressures, as shown in Figure 9. After data point fitting regression analysis, K_c = 1.5 and K_c = 2.0, and the normalised pore-water pressure development curve conforms to the development law of power function as follows:

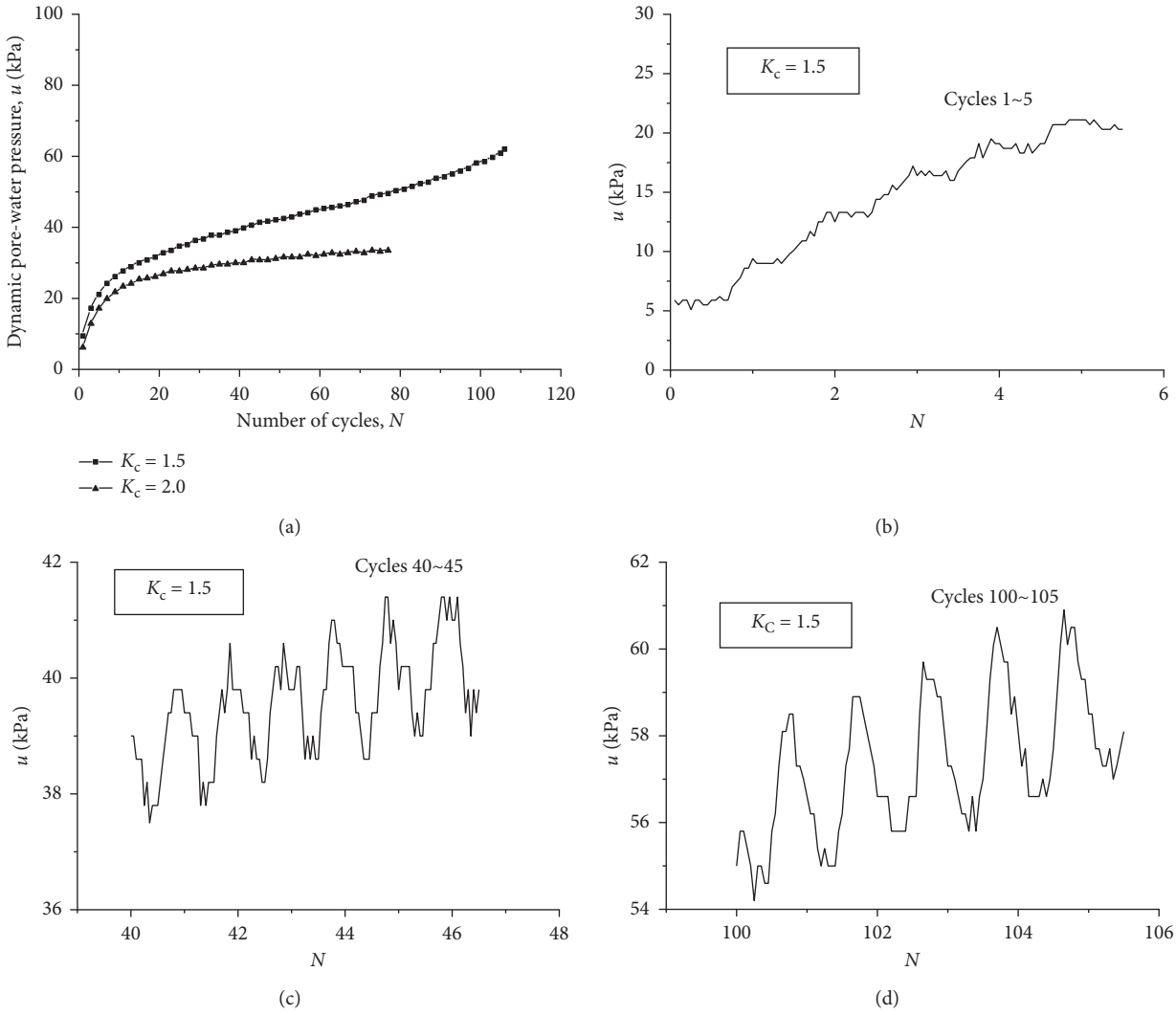

Figure 6: Development of u at three stages (K_c = 1.5). (a) u against N curves under different K_c values. (b) First stage. (c) Second stage. (d) Third stage.

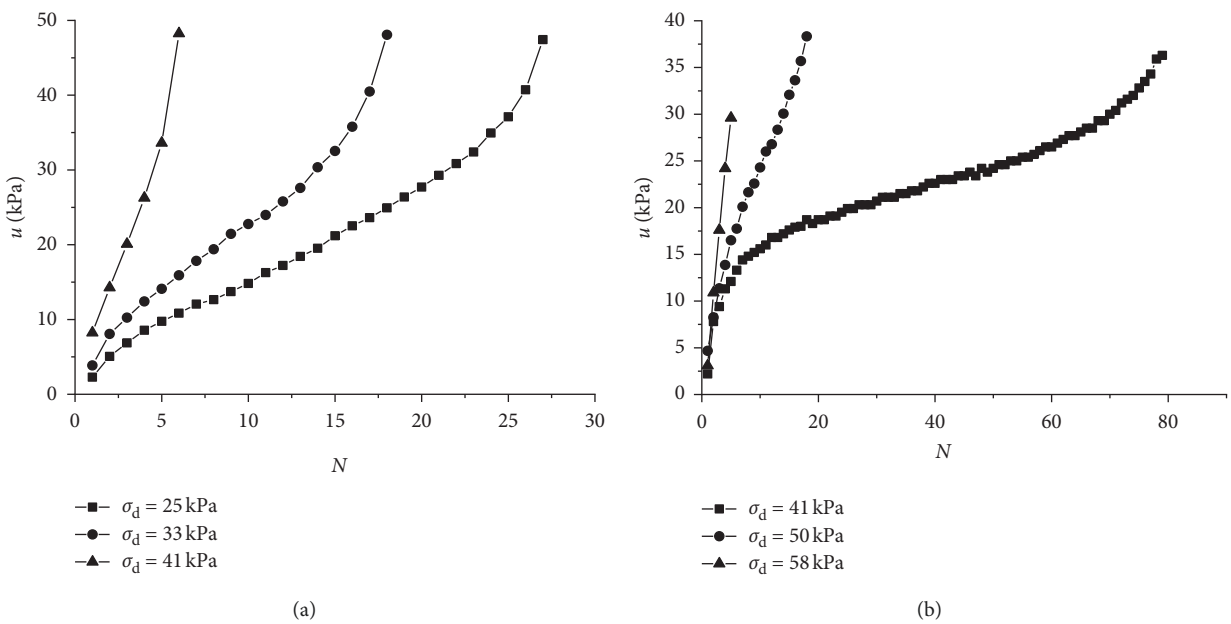

Figure 7: Continued.

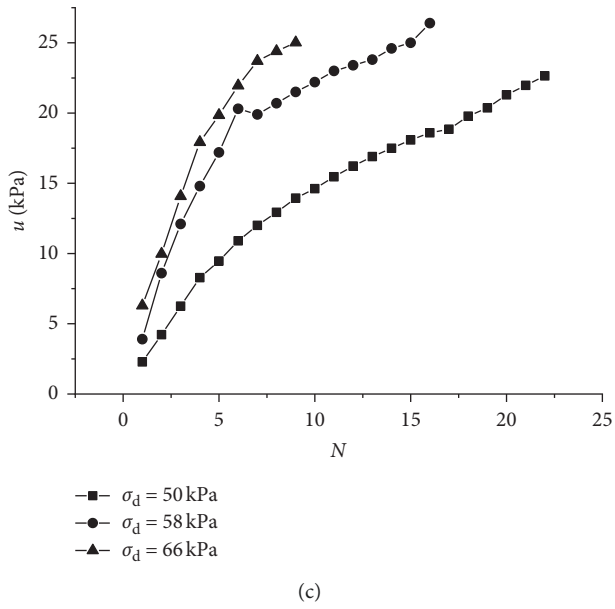

(c)

Figure 7: Relationship curve between u and N under different dynamic stresses. (a) K_c = 1.0. (b) K_c = 1.5. (c) K_c = 2.0.

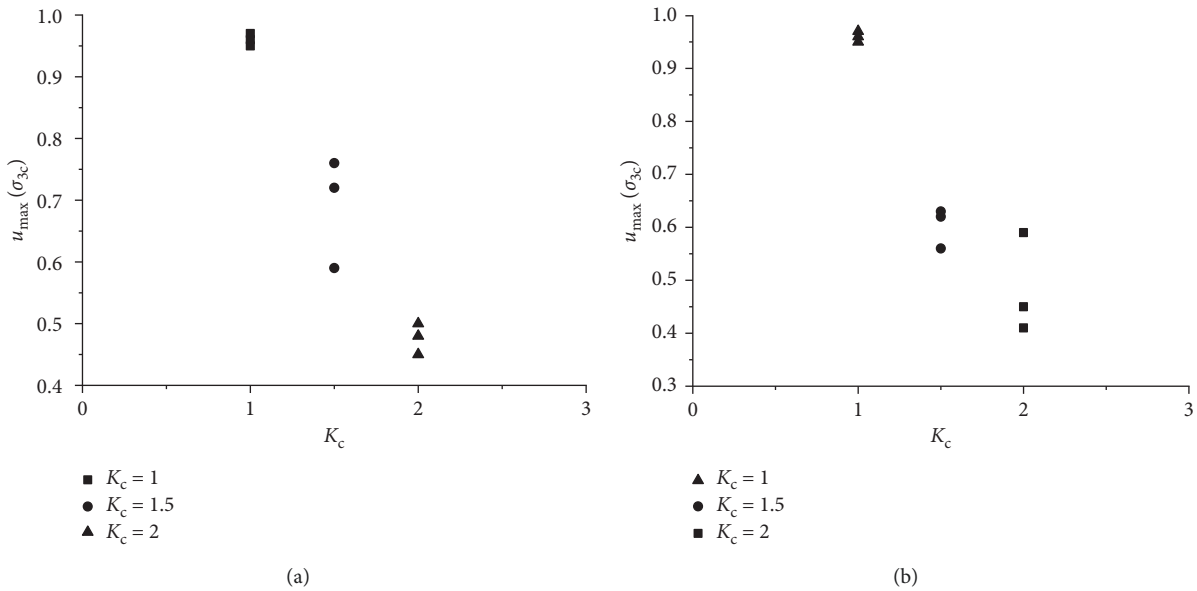

(a) (b)

Figure 8: Continued.

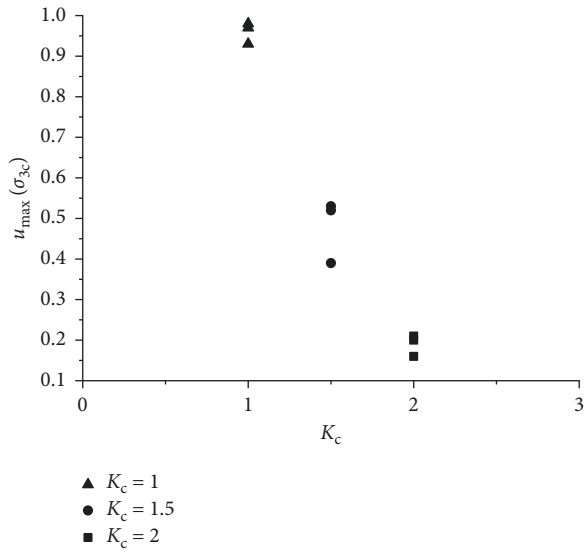

(c)

Figure 8: Relationship curve between u_{max}/σ_{3c} and K_c.

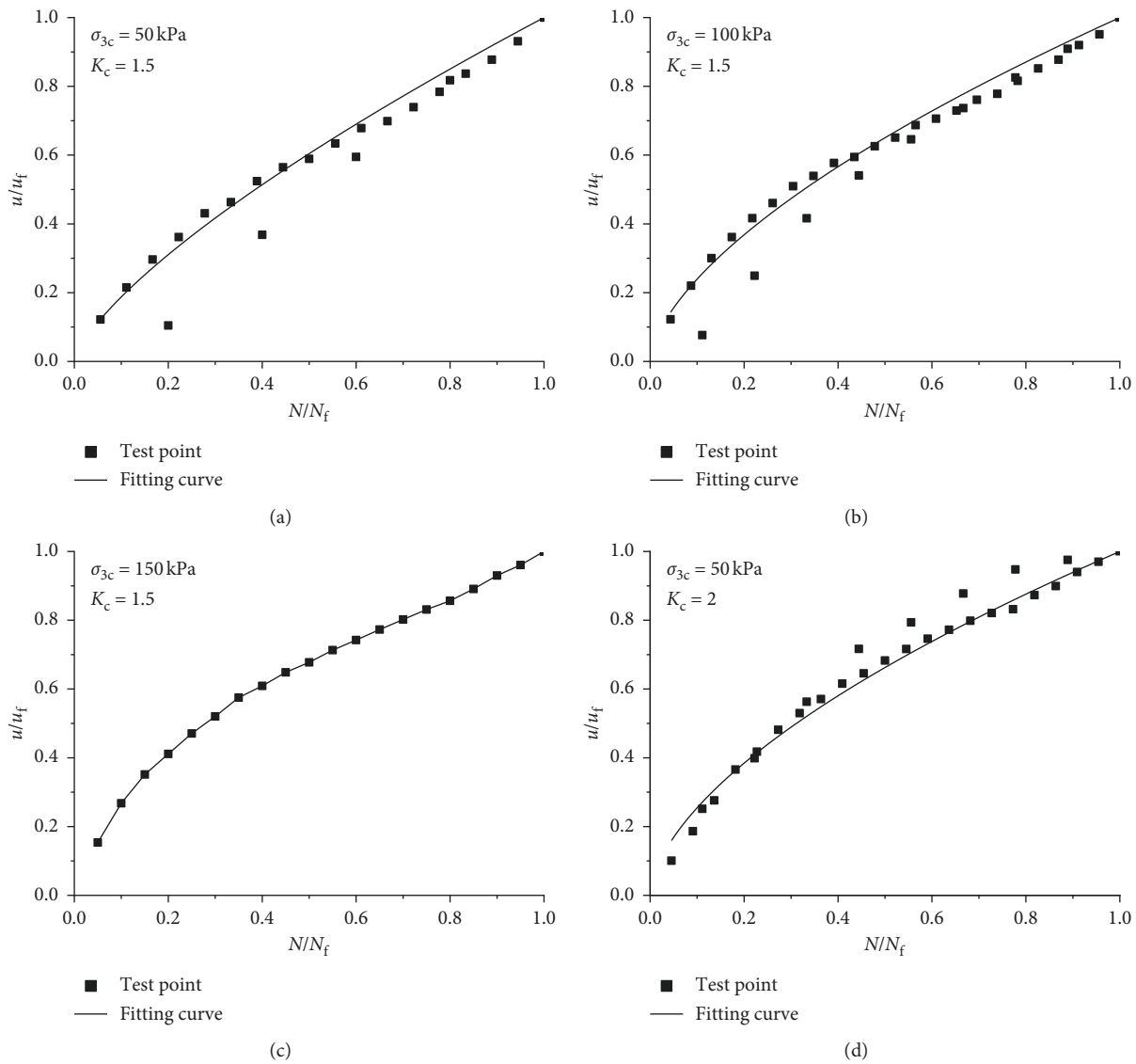

Figure 9: Continued.

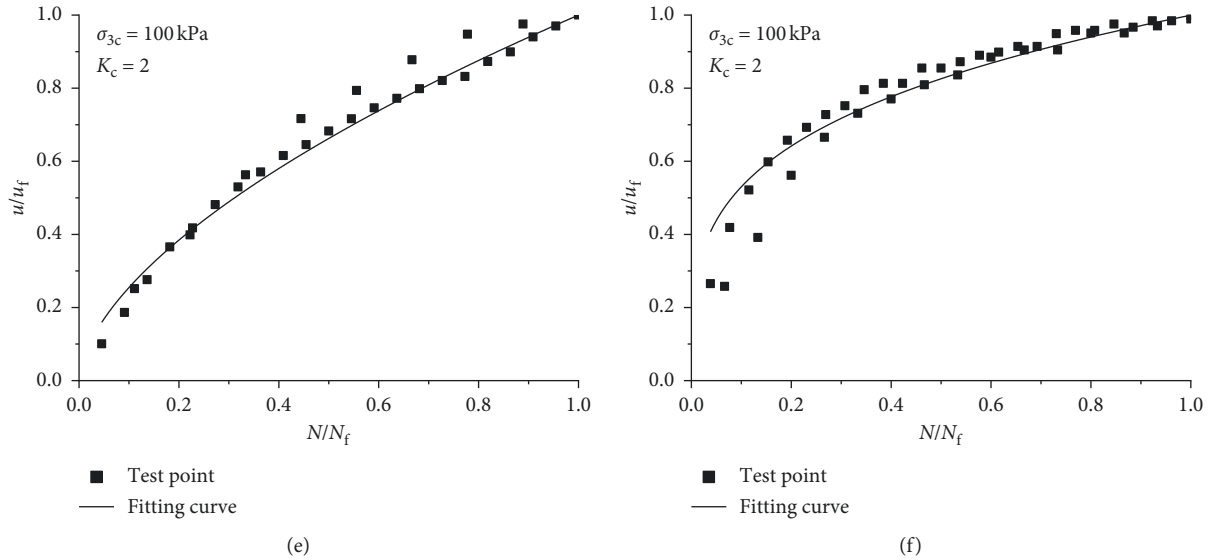

Figure 9: Normalised relationship curve between u/u_f and N/N_f.

$$\frac{u}{u_f} = \left(\frac{N}{N_f}\right)^{1/\alpha}. \quad (2)$$

In the case of different initial shear stresses, the power series is used to fit the pore-water pressure growth model, and the experimental data points are subjected to regression analysis. The corresponding fitting curves are provided.

Table 3 presents the parameters of the pore-water pressure development model under different initial shear stresses. At K_c = 1.5, the confining pressure has no effect on the parameter α. At K_c = 2.0, the power function model parameter α increases with the increase of confining pressure.

Table 3: Model parameters of pore-water pressure development under different initial shear stresses.

Consolidation ratio	1.5	2
Model	Power function model	
Confining pressure (kPa)	Parameter α	Parameter α
50	1.7	1.68
100	1.6	3.62
150	1.7	4.30

3.3. Effects of Vibration Frequency on the Dynamic Pore-Water Pressure Characteristics of Saturated Sand. Figure 10 shows the development curve of the dynamic pore-water pressure with the number of cycles under different dynamic stresses during isotropic consolidation. After the cyclic load is applied, the pore-water water pressure of the sand increases rapidly in the initial stage, and then, the growth rate slows down and stabilises. Finally, the pore-water pressure reaches a certain level and then rapidly increases to the confining pressure. The accumulation law of pore-water pressure is the growth mode of "quick-stable-intensified." The greater the dynamic stress, the steeper the curve, and a short time is needed to achieve liquefaction damage. The lower the dynamic stress, the smoother the curve and the higher the number of cycles required for the liquefaction damage.

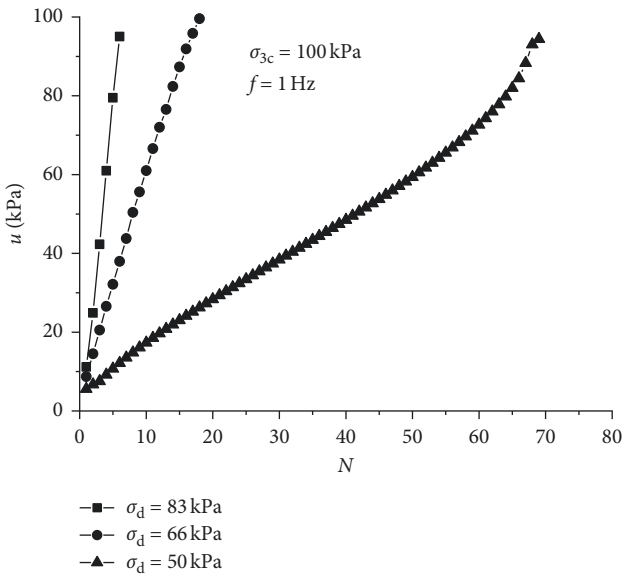

Figure 10: Relationship between u and N under different dynamic stresses.

Figure 11 shows a fitting curve of the vibration pore-water pressure with the number of cycles at different frequencies during isotropic consolidation. At first, the dynamic pore-water pressure increases gradually, and the curve is convex. When the sample is close to the initial liquefaction, that is, N/N_f is over 0.8, the pore-water pressure and the growth rate of pore-water pressure ratio increases rapidly, so the sample quickly reaches liquefaction. The test is stopped after the sample is destroyed. Furthermore, the state of the relationship curve is the same within the range of the test frequency and confining pressure, indicating that the

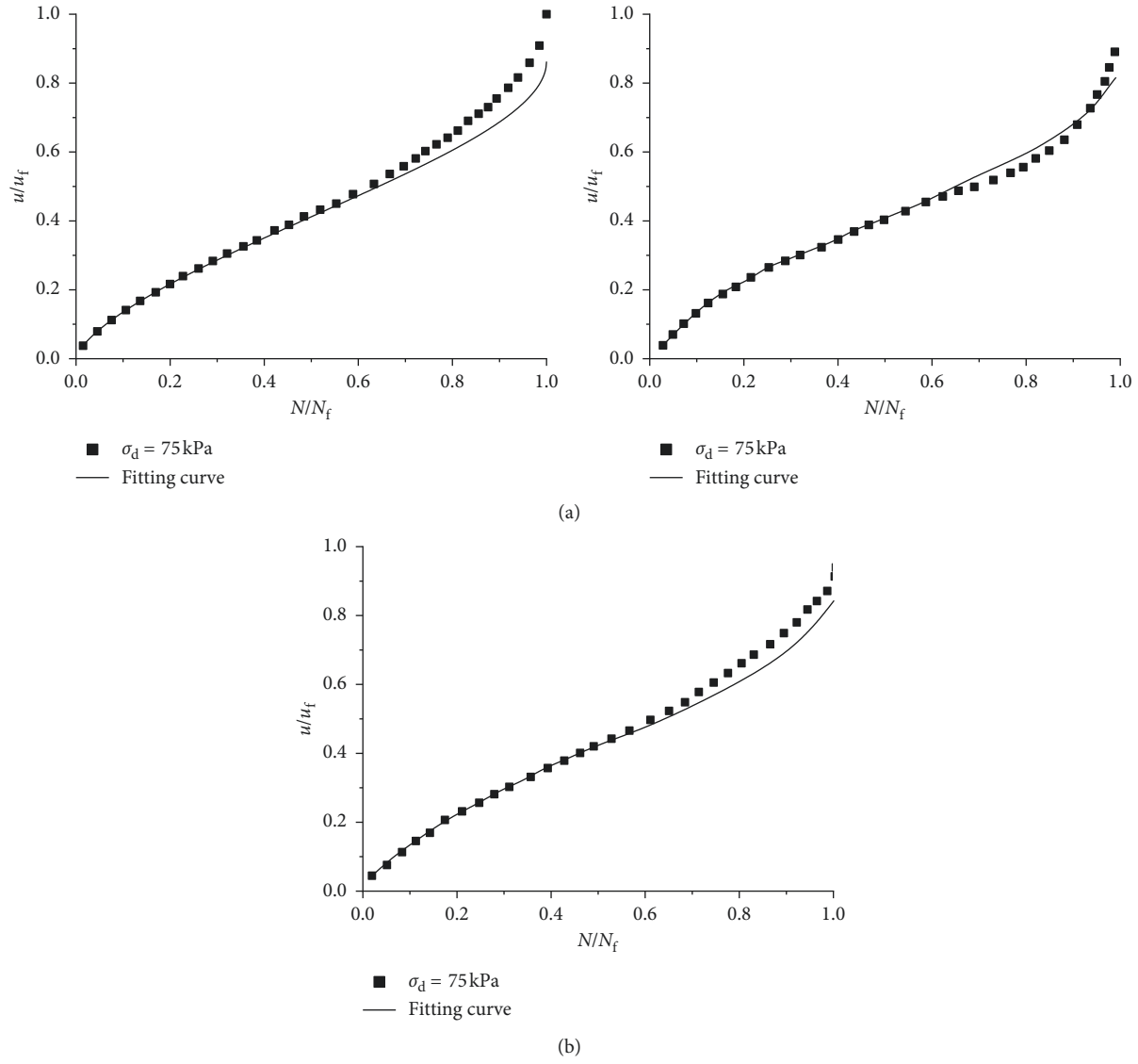

Figure 11: Development mode between u/u_f and N/N_f.

growth law of the dynamic pore-water pressure is the same under different vibration frequencies.

3.4. Pore-Water Pressure Development Model considering Vibration Frequency. Figure 11 displays the fitting curve of the test constant θ with the vibration frequency. The fitting results indicate that the test constant θ is almost linear with the vibration frequency in the vibration frequency range of 1–3 Hz, as shown in Table 4.

A pore-water pressure development model that considers vibration frequency is proposed on the basis of the Seed pore-water pressure development model:

$$\frac{u}{\sigma_0'} = \frac{2}{\pi}\arcsin\left(\frac{N}{N_L}\right)^{1/2\theta(f)}, \quad (3)$$

where θ is the function of the vibration frequency f from 1 Hz to 3 Hz, and $\theta(f) = 0.01f + 0.73$.

Table 4: Values of test constant θ.

Frequency (Hz)	1	2	3
θ	0.74	0.75	0.76

Figure 12 presents a fitting curve of the vibration pore-water pressure ratio with the number of cycles at the same vibration frequency (f = 1 Hz) and different confining pressures (σ_{3c}) and dynamic stresses (σ_d) under isotropic consolidation.

Figure 13 presents a fitting curve of the pore-water pressure ratio with the number of cycles at the same confining pressure (σ_{3c}) and dynamic stress (σ_d) and different vibration frequencies (f = 1, 2, and 3 Hz) under isotropic consolidation.

Table 5 shows that θ under different frequencies, confining pressures, and dynamic stresses can be obtained from

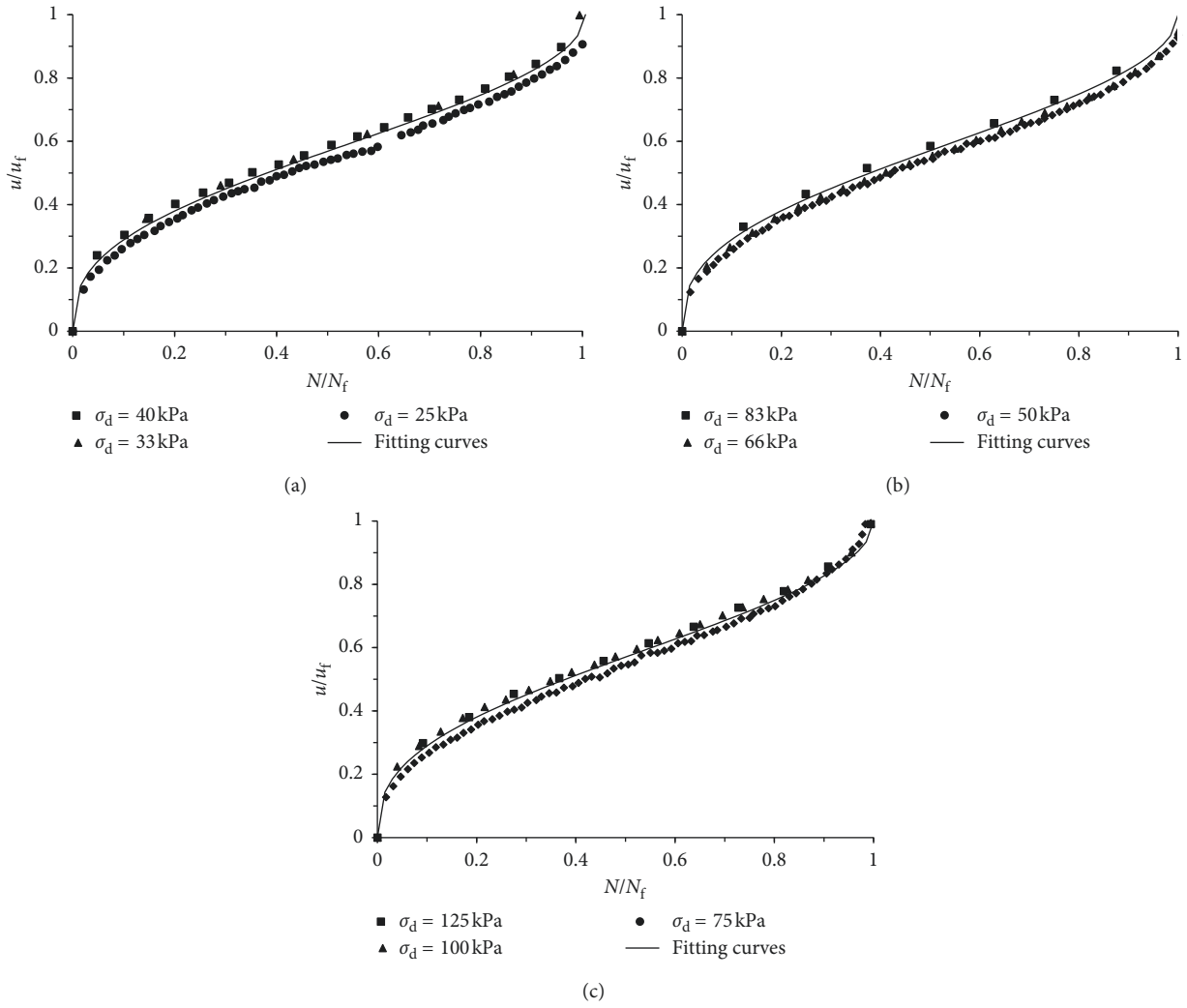

Figure 12: Development modes between u/u_f and N/N_f under different confining pressures and dynamic stresses.

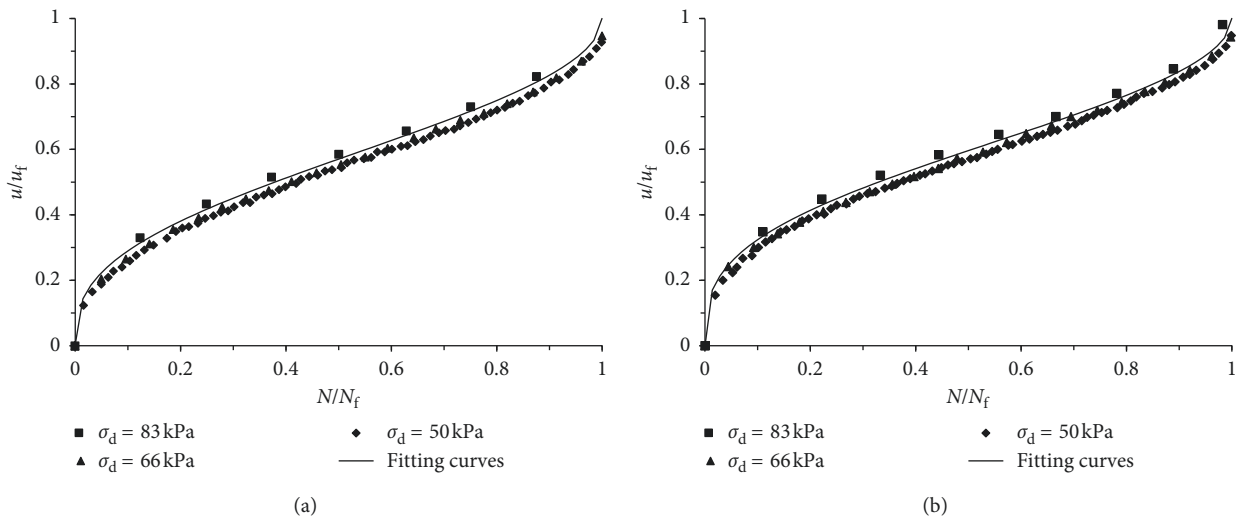

Figure 13: Continued.

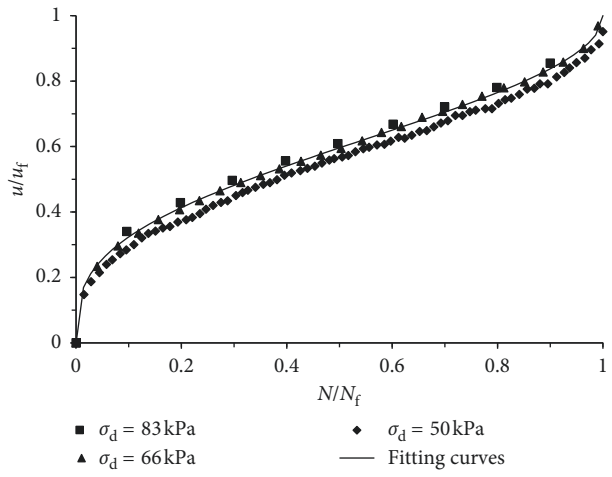

(c)

Figure 13: Development modes between u/u_f and N/N_f under different frequencies and dynamic stresses.

Figures 12 to 13. Under isotropic consolidation, when the vibration frequency remains the same, θ does not change with the confining pressure and dynamic pressure but changes linearly only as the frequency changes.

4. Conclusions

The pore-water pressure characteristics of saturated sand in the Wenchuan area were studied through the dynamic triaxial test system. The influence of initial shear stress and vibration frequency on the development mode of the dynamic pore-water pressure of sand was discussed, and the model of the dynamic pore-water pressure of saturated sand considering vibration frequency was established. The research shows the following:

(1) Under different initial shear stresses, the development of the dynamic pore-water pressure of saturated sand is different. The larger the initial shear stress, the slower the development curve of the pore-water pressure and the higher the number of cycles required to reach the same pore-water pressure. For the same number of cycles, the smaller the initial shear stress, the larger the dynamic pore-water pressure.

(2) When the initial shear stress exists, the dynamic pore-water pressure cannot develop to the confining pressure as the cycle time increases. The larger the initial shear stress, the smaller the dynamic pore-water pressure when the sample is destroyed. The maximum pore-water pressure ratio decreases linearly with the increase of consolidation ratio.

(3) The normalised dynamic pore-water pressure and failure time of vibration curves are consistent with the development law of power function, and the power function model parameters are affected by initial shear stress and confining pressure.

(4) Under isotropic consolidation, the accumulation law of the pore-water pressure of saturated sand is the growth mode "fast-stable-intensified." The greater the dynamic stress, the steeper the curve, and a short time is needed to achieve liquefaction damage. The lower the dynamic stress, the smoother the curve and the greater the number of cycles required for liquefaction. The growth law of the dynamic pore-water pressure at different vibration frequencies is the same.

(5) A pore-water pressure correction model that considers vibration frequency is proposed on the basis of the Seed pore-water pressure development model, and the test parameters are concluded to be linear with the vibration frequency.

(6) Under isotropic consolidation, when the vibration frequency remains the same, θ does not change with the confining pressure and dynamic stress but changes linearly only as frequency changes.

Table 5: θ under different frequencies, confining pressures, and dynamic stresses.

Frequency (Hz)	Confining pressure (kPa)	Dynamic stress (kPa)	θ
f = 1.0	50	41/33/25	0.74
	100	83/66/50	
	150	125/100/75	
f = 2.0	50	41/33/25	0.75
	100	83/66/50	
	150	125/100/75	
f = 3.0	50	41/33/25	0.76
	100	83/66/50	
	150	125/100/75	

Data Availability

The data used to support the findings of this study are included within the article.

Conflicts of Interest

The authors declare that there are no conflicts of interest regarding the publication of this paper.

Acknowledgments

The authors are grateful for the financial support from the National Natural Science Foundation of China (No. 51709145) and the Scientific Research Foundation of Nanjing Institute of Technology (YKJ201727).

References

[1] A. Lashkari, A. Karimi, K. Fakharian, and F. Kaviani-Hamedani, "Prediction of undrained behavior of isotropically and anisotropically consolidated Firoozkuh sand: instability and flow liquefaction," *ASCE International Journal of Geomechanics*, vol. 17, no. 10, article 04017083, 2017.

[2] A. B. Fourie and L. Tshabalala, "Initiation of static liquefaction and the role of K_0 consolidation," *Canadian Geotechnical Journal*, vol. 42, no. 3, pp. 892–906, 2005.

[3] T. Wichtmann and T. Triantafyllidis, "Influence of the grain-size distribution curve of quartz sand on the small strain shear modulus gmax," *Journal of Geotechnical and Geoenvironmental Engineering*, vol. 135, no. 10, pp. 1404–1418, 2009.

[4] Y. Yilmaz and M. Mollamahmutoglu, "Characterization of liquefaction susceptibility of sands by means of extreme void ratios and/or void ratio range," *Journal of Geotechnical and Geoenvironmental Engineering*, vol. 135, no. 12, pp. 1986–1990, 2009.

[5] D. Wijewickreme and Y. P. Vaid, "Experimental observations on the response of loose sand under simultaneous increase in stress ratio and rotation of principal stresses," *Canadian Geotechnical Journal*, vol. 45, no. 5, pp. 597–610, 2008.

[6] D. Porcina, G. Garidi, and V. N. Ghionna, "Undrained monotonic and cyclic simple shear behavior of carbonate sand," *Geotechnique*, vol. 58, no. 8, pp. 635–644, 2008.

[7] H. D. Dief and J. L. Figueroa, "Liquefaction assessment by the unit energy concept through centrifuge and torsional shear tests," *Canadian Geotechnical Journal*, vol. 44, no. 11, pp. 1286–1297, 2007.

[8] Z. X. Yang, X. S. Li, and J. Yang, "Undrained anisotropy and rotational shear in granular soil," *Geotechnique*, vol. 57, no. 4, pp. 371–384, 2007.

[9] Y. P. Vaid, J. D. Stedman, and S. Sivathayalan, "Confining stress and static shear effects in cyclic liquefaction," *Canadian Geotechnical Journal*, vol. 38, no. 3, pp. 580–591, 2001.

[10] I. Towhata and K. Ishihara, "Shear work and pore water pressure in undrained shear," *Soils and Foundations*, vol. 25, no. 3, pp. 73–84, 1985.

[11] H. B. Seed and I. M. Idriss, "Pore-water pressure changes during soil liquefaction," *Journal of the Geotechnical Engineering Division, ASCE*, vol. 102, no. 4, pp. 323–346, 1976.

[12] H. B. Seed and L. F. Harder, "SPT-based analysis of cyclic pore pressure generation and undrained residual strength," in *Proceeding of H.B.Seed Memorial Symposium*, pp. 351–376, University of California Berkeley, Berkeley, California, 1990.

[13] S. Kato, K. Ishihara, and I. Towhata, "Undrained shear characteristics of saturated sand under anisotropic consolidation," *Soils and Foundations*, vol. 41, no. 1, pp. 1–11, 2001.

[14] J. Yang and H. Y. Sze, "Cyclic behaviour and resistance of saturated sand under non-symmetrical loading conditions," *Geotechnique*, vol. 61, no. 1, pp. 59–73, 2011.

[15] S. Sivathayalan and D. Ha, "Effect of static shear stress on the cyclic resistance of sands in simple shear loading," *Canadian Geotechnical Journal*, vol. 48, no. 10, pp. 1471–1484, 2011.

[16] V. N. Georgiannou and M. Konstadinou, "Effects of density on cyclic behaviour of anisotropically consolidated Ottawa sand under undrained torsional loading," *Geotechnique*, vol. 64, no. 4, pp. 287–302, 2014.

[17] G. Suazo, A. Fourie, J. Doherty, and A. Hasan, "Effects of confining stress, density and initial static shear stress on the cyclic shear response of fine-grained unclassified tailings," *Geotechnique*, vol. 66, no. 5, pp. 401–412, 2016.

[18] K. Pan and Z. X. Yang, "Effects of initial static shear on cyclic resistance and pore pressure generation of saturated sand," *Acta Geotechnica*, vol. 13, no. 2, pp. 473–487, 2018.

[19] Z. X. Yang and K. Pan, "Flow deformation and cyclic resistance of saturated loose sand considering initial static shear effect," *Soil Dynamics and Earthquake Engineering*, vol. 92, pp. 68–78, 2017.

[20] Y. F. Gao, J. Zhang, and Y. Shen, "Characteristics of pore water pressure of saturated silt under wave loading," *China Ocean Engineering*, vol. 24, no. 1, pp. 161–172, 2010.